Validation of SMOS brightness temperatures during the HOBE Airborne Campaign, Western Denmark

Simone Bircher, J.E. Balling, N. Skou, Yann H. Kerr

SMOS Validation by means of an airborne campaign in the Skjern River Catchment, Western Denmark

Journal:	*Transactions on Geoscience and Remote Sensing*
Manuscript ID:	TGRS-2011-00225
Manuscript Type:	Soil Moisture and Ocean Salinity Mission 2010 Special Issue paper
Keywords:	Soil, Water, Remote sensing, Microwave radiometry

SMOS Validation by means of an airborne campaign in the Skjern River Catchment, Western Denmark

Simone Bircher, Jan E. Balling, Niels Skou, *Fellow, IEEE* and Yann Kerr, *Senior Member, IEEE*

Abstract

The Soil Moisture and Ocean Salinity Mission (SMOS) delivers global surface soil moisture fields at high temporal resolution which is of high relevance for water management and climate predictions. For data validation, an airborne campaign with the L-band radiometer EMIRAD-2 and concurrent ground sampling was carried out within one SMOS pixel in the Skjern River Catchment, Denmark. By means of this dataset the objective of this study is a step-wise comparison of brightness temperatures from point via air- to spaceborne (SMOS) scale. From soil moisture samples brightness temperatures were estimated through the L-band Microwave Emission of the Biosphere (L-MEB) model with land-cover specific model settings. A simple uncertainty assessment by means of a set of model runs with parameters varied within a most likely interval resulted in a considerable range of brightness temperatures. Under certain constellations the ground data was in good agreement with EMIRAD. Likewise was the latter in accordance with SMOS data. The comparison of more sophisticated upscaling by means of air- and spaceborne weighting functions and a simple mean showed no significant change. Small temporal variability in soil moisture conditions and RFI-prone SMOS data throughout the campaign limited the extent of the validation work. Further attempts over longer time frames are planned by means of soil moisture network data as well as studies on the impacts of organic layers under natural vegetation and higher open water fractions at surrounding grid nodes.

Index Terms

Passive microwaves, soil moisture, SMOS, L-band, L-MEB, airborne campaign, validation.

I. Introduction

Soil moisture is one of the key state variables in water balance. As it constitutes the main water source for vegetation and also significantly impacts water and energy exchanges at the land-surface-atmosphere interface

S. Bircher, J. E. Balling and N. Skou are with the Department of Microwaves and Remote Sensing, DTU Space, Technical University of Denmark, 2800 Kgs. Lyngby, Denmark e-mail: subi@space.dtu.dk.

Y. Kerr is with the Centre d'Etudes Spatiales de la Biosphère (CESBIO), 31401 Toulouse, France.

Manuscript received April 19, 2005; revised January 11, 2007.

improving our understanding on its behavior is highly relevant for water resources and crop management, weather forecasts, climate predictions and hazard analysis. Many authors, e.g. [1]–[3] have reported that soil moisture is highly variable both in space and time and across scales as a result of (1) spatially variable land surface properties, (2) seasonal and spatially variable climatic forcings, and (3) anthropogenic influences. The above render soil moisture highly difficult to assess and one of the major uncertainties in climate/meteorological and hydrological models. Thus, reliable soil moisture data at global spatial scale and with high temporal resolution is urgently needed.

The Soil Moisture and Ocean Salinity Mission (SMOS) [4] launched on November 2, 2009 has the goal to deliver the first global surface soil moisture fields at a temporal resolution of 3 days by means of a spaceborne passive L-band (1.4 GHz) microwave imaging radiometer with aperture synthesis. This technique is currently believed to be most effective [5], [6] as in the low frequency domain (1) a large contrast between the dielectric properties of liquid water and dry soil and (2) minimal signal attenuations by atmosphere, vegetation and surface roughness facilitate the separation of a soil's water content from the other components, the latter being further supported by the instrument's full polarization and multi-angle measurement configuration. Drawbacks are a signal origin depth of around 5 cm (and even less under wet conditions) [7], [8] and the low spatial resolution of approximately 40-50 km refered to 'SMOS pixel' hereafter.

SMOS soil moisture data (L2 product) is iteratively retrieved for each node of a fixed grid by minimizing the deviation between SMOS brightness temperatures (L1C product) and brightness temperatures simulated by means of an aggregated version of the L-band Microwave Emission of the Biosphere (L-MEB) model [9], [10]. More details on the SMOS measurement principal and the L-MEB model will be given in sections II-B3 and III-A, respectively.

After a half year commissioning phase following the launch SMOS was declared as performing according to expectations and the data considered sufficiently good for distribution. One of the remaining problems is linked to spurious signals due to radiofrequency interference (RFI) which turned out to be much larger and more frequent than expected [11]–[14].

At this stage an important step of the mission is data validation in different climatic regions with variable environmental conditions. Based on results from SMOS data comparison with in-situ measurements the soil moisture retrieval algorithm will be improved (better models) and data reprocessed in order to continuously improve SMOS product quality. Currently, such validation activities are carried out in many parts of the world [15].

Due to the high spatial and temporal variability of soil moisture across scales the validation of satellite soil moisture products is complicated by the mismatch in scale between the large satellite footprints and point measurements on the ground [16]. One approach that has been widely used to attain the required data for satellite validation is the performance of short-term intensive field campaigns with concurrent airborne and ground measurements at the time of the satellite overpass, e.g. [17]–[22]. This offers the advantage of a stepwise validation across spatial scales which can be carried out directly at brightness temperature level. In representative areas of the satellite footprint selected airborne footprints with a spatial resolution in the order of few kilometers are validated with an average value of brightness temperatures modeled from densely spaced ground samples by means of a forward model. In a second step, the average value of the airborne data covering an adequate fraction of the satellite footprint is

compared to the satellite product.

With respect to the forward model, L-MEB has been widely applied in such studies. As it is constructed by means of several fitting parameters whose settings can significantly alter the resulting brightness temperature output, many previous investigations have focused on the retrieval of best-fit parameters for limited areas of various types of fairly homogeneous land cover conditions (e.g. [23]–[29]).

Airborne campaigns were carried out in different climatic regions in connection with the preparation of the SMOS mission and continue to constitute a core activity in SMOS calibration and validation, e.g. arid climate, southeastern Australia: [21], [22], [30]; temperate zone, Upper Danube, Rur- and Erft Catchments, Germany: [31]–[33], southwestern France: [34], Arctic, northern Finland: [35]. One campaign took place in the Skjern River Catchment, Denmark, between April 26 and May 9, 2010, within the framework of the Danish Hydrological OBservatory and Exploratorium (HOBE, www.hobe.dk) [36]. It included four flights during SMOS overpass with the L-band radiometer EMIRAD-2 [37], [38] on board, simultaneous surface soil moisture measurements of the mineral as well as the organic layers within three patches of differing land cover, and the assessment of vegetation and surface roughness data at the beginning and the end of the campaign.

The importance to validate SMOS data at the Danish site is twofold. First, it complements the other SMOS Cal/Val regions in that it is Europe's northernmost intensely cultivated area with features related to the prevailing environmental conditions at this latitude such as sandy soils with large organic deposits under natural vegetation and region-specific land cover such as heathland. Secondly, the area is located at short distance to the coast line in two directions which enables studies of the impact of open water on the SMOS data quality. Advantages of this site are furthermore temporally increased data acquisition frequency and less data contamination by RFI compared to more southern regions as well as its pronounced flatness.

The main objective of this article is to present the step-wise validation of one selected SMOS pixel over spatial scales from point (ground data modelled by means of L-MEB) to intermediate (EMIRAD-2) to large (SMOS) scale at top of atmosphere brightness temperature level (TOA L1C, H and V polarization) by means of the HOBE campaign dataset. In contrast to the above-mentioned previous parameter-retrieval studies, the approach followed here is to base the choice of model parameters on knowledge from these earlier studies as well as parameterizations using our own campaign field measurements together with relations from literature. Thereupon, a most likely value range for each of the most important model parameters is defined for all encountered land cover types and applied to each individual ground soil moisture sampling point. This approach allows to account for the influence of parameter uncertainties on the resulting brightness temperatures. Moreover, we investigate the benefit of a more sophisticated upscaling through weighted averaging by means of the instrument antenna pattern over a simple averaging approach at both airborne and spaceborne scale.

In this study only ground soil moisture data from the mineral soils are considered and a SMOS pixel virtually free of open water is chosen. Resulting knowledge on parameter choices and uncertainties create a foundation for future investigations that will address the pecularities of this SMOS validation site, namely the open water impact and the influence of organic matter.

II. Data

A. Description of validation site

The SMOS pixel around grid node 2002029 (55.957 N, 9.131 E) was chosen for validation as it exhibits minimal open water fraction while covering a substantial part of the Skjern River Catchment (Fig. 1a+b). The entire catchment comprises an area of approximately 2500 km^2 and is situated in Mid-Jutland, Western Denmark. The climate in the region is temperate-maritime with winter and summer mean temperatures of around 2 and 16 $^{\circ}C$, respectively, and annual precipitation between approximately 800 to 900 mm [39]. The eastern edge of the validation site is situated at the original margin of the ice sheet during the last glacial advance exhibiting a hilly landscape with mainly loamy soils on calcareous tills while the major part comprises the primal fluvioglacial outwash plain consisting of low-relief sandy sediments [40]. The predominant naturally occurring soil type is podsol covered by a pronounced poorly decomposed raw humus layer. Nearly 80% of the land is under intensive mechanized agricultural practice (mainly winter/spring barley, potatoes and grass), intermixed with patches of forest plantations (mostly spruce with scarce understory and moss-covered ground surface, ca. 10%), as well as heath/grassland (primarily scotch heather bushes with a herbal layer and dry natural grass) and wetlands (ca. 6%). The area is sparsely populated with scattered farms and single villages.

The catchment is well-covered with climate stations and rain gauges operated by the Danish Meteorological Institute (DMI). HOBE is maintaining four study sites where all components of the water cycle are assessed [41] and in autumn 2009 a soil moisture network was established within the SMOS validation area (Fig. 1b). The network includes 30 stations which are spatially distributed according to respective fractions of prevailing land cover and soil types and aligned along the 30-year mean annual precipitation gradient of the area [42]. Per station, soil moisture, temperature and electrical conductivity measurements in the 0-5 cm, 20-25 cm and 50-55 cm depth ranges of the mineral soil are logged at 30 minutes intervalls.

B. HOBE airborne campaign

The HOBE airborne campaign [36] took place between April 26 and May 9. 2010. Four 3-hour flights (April 29, May 2, 4, and 9) were carried out centered around SMOS ascending overpass at approximately 6.30 local time. Simultaneously, intense ground measurements were undertaken within three 2x2 km patches selected according to the area's most representative land covers, namely agriculture, heath/grassland and forest (Fig. 1c-e). Within the agriculture patch, apart from the winter barley and grass patches most fields were under cultivation and still of bare appearance.

1) Ground data: Soil moisture measurements were carried out with hand-held Delta T ML2x ThetaProbes [1] (0-6 cm depth). The forest and heath patches were sampled on the first three, the agricultural patch on all four days. Sampling time was about 4-6 hours roughly centered around SMOS overpass. Altering spatio-temporal soil moisture conditions during the sampling time slot were not discovered. Fig. 1c-e illustrates the respective sampling

[1]Mention of manufacturers is for the convenience of the reader only and implies no endorsement on the part of the authors

patterns. On the agricultural patch along 6 north-south transects each 50 m 3 probe readings were recorded from the top of the mineral soil. On the heath and forest patches the sampling spacing was enlarged to 200 m as per location additionally 3 readings were acquired from the top of the 5-20 cm thick moss/organic layer. Gravimetric samples were taken at 15 locations per patch in case of the mineral soil, and additionally at 33 locations in case of the moss/organic layer on the heath and forest patches. For each sampling point land cover type, vegetation height and (where applicable) crop row orientation were recorded.

Sensor- and site-specific linear calibration curves (for each sensor individually/all sensors together) were derived in the lab over the entire wetness range using mineral surface soil samples from the three patches, and validated by means of the field gravimetric samples (Fig. 2). All campaign probe readings were recalculated using the respective sensor-specific calibration curves or the site-specific where the sensor id was not applicable. Average values for all respective campaign dates and patches are compiled in Table I.

Soil bulk density estimated by means of the collected soil samples revealed average values (standard deviations) of 1.21(0.16), 1,31(0.16) and 1.34(0.18) g/cm^3 for agriculture, forest and heath, respectively. With respect to soil texture, sand- and clay fractions within all three patches are in the order of 0.75-1.0 and 0.0-0.05 according to the Danish topsoil grid [40], while site-specific texture analysis of the campaign samples revealed less sandy conditions with sand- and clay fractions between 0.39-0.89 and 0.02-0.18, respectively.

At the beginning and towards the end of the campaign (April 28 and May 6) destructive vegetation sampling was carried out on the agriculture and heath at around 8 locations per patch. A significant increase in average vegetation water content between the two measurement dates was observed for all vegetation types except in case of the agricultural grass where only one sample was available per measurement day (Table II).

Within the agriculture patch 3 m transects of surface roughness were measured in both N-S and E-W direction on two freshly plowed and sown spring barley fields and two freshly planted potato fields with pronounced row structure - the conditions assumed to exhibit least/most distinct roughness characteristics. The respective root mean square deviations from the average measured heights over all available profiles per land cover class are listed in Table III. Within the heath and forest patches roughness measurements were omitted as it was not possible to remove the present moss- and vegetation covers without heavily disturbing the surface.

2) Airborne data (EMIRAD-2): The airborne measurements were acquired by means of the L-band radiometer EMIRAD-2 at incidence angles of 0 and 40° and both, H and V polarization, respectively, and integrated to 1 msec. A detailed description of the instrument can be found in [37], [38]. On each sampling day 10 north-south tracks were flown over the validation site in such a manner that a maximum number of soil moisture network stations and the dense snapshot sampling patches were covered (Fig. 1b). For all flights the altitude was kept at 2000 m corresponding to an approximate -3 dB swath of 1.4 km. Average EMIRAD data coverage of the SMOS pixel and the 2x2 km ground sampling patches was around 35 and 75%, respectively, and fairly consistent for 0 and 40° antennas and on all flight dates (Fig. 3a-c).

In addition to standard internal calibration, external calibration was conducted by means of liquid nitrogen as well as over open water in the Ringkøbing Fjord at the beginning of each flight. Data checks revealed a systematic

offset of around 3.5 K from the expected value in the 40° V-polarization antenna. This bias must be caused from an unknown external source and has not been corrected for.

A preliminary RFI filtering scheme was applied to the data. Based on [43] measurements with kurtosis ratios outside the mean +/-4 standard deviation interval from an RFI-free signal were flagged as RFI-contaminated (RFI-%). In addition, RFI-flags were set for all brightness temperature measurements above 300 K and/or with 3rd and 4th Stokes parameter values outside the +/-10 K range. The RFI-% in the EMIRAD data was low throughout all flight dates (in the order of 3-5% of all samples within the SMOS pixel).

The EMIRAD data was georeferenced by means of the onboard GPS and inertial navigation system (EGI) to determine the locations of the antenna boresights and associated extents of the -3 dB footprints, and the SRTM digital elevation model [44] for conversion of aircraft altitude to height assuming a flat earth. Effects of polarization mixing caused by aircraft attitude have subsequently been removed from the datasets.

3) Spaceborne data (SMOS): In this study, exclusively L1C brightness temperature data from ascending overpass on days with airborne measurements was considered. For comparison with the EMIRAD data, the L1C data was previously transferred from antenna to Top Of Atmosphere (TOA) level (XY to HV) by applying the Farraday rotation. Unfortunately, despite of the fact that the northern latitudes are generally less RFI-prone, out of the four sampling days, three were heavily contaminated so that only the dataset from May 02 could be used for validation. The fact that SMOS is a complex interferometer measuring from very large distances and thus looking at large areas including land, water and sky contributions at once, explains why the system can encounter RFI-problems while EMIRAD-2 data remains nearly unaffected at the same time.

For soil moisture computation the SMOS L1C data is resampled to a fixed earth surface grid with approximately 15 km spacing, but the actual data used for the retrieval at each grid node originates from an area spanning approximately 123 km ('working area') in diameter integrating the signal observed at a range of incidence angles from about 0-60 ° and different view directions. However, the received signal power is weighted by the shape of the SMOS antenna pattern [10] so that the major portion originates from the innermost 40-50 km (SMOS 'pixel'). Fig. 1a shows the SMOS grid and the corresponding 123 and the 44 km areas around the selected node 2002029 to be validated in the Skjern River Catchment. For the entire area the open water fraction is in the order of 1% (based on several land cover classifications with differing spatial resolutions, i.e. LANDSAT 30 m, CORINE2000 100 m, ECOCLIMAP 1 km), and given that most water bodies are situated at the margin of the 123 km area, even smaller in case of the radiometric fraction considering the antenna weighting function.

III. Methods

A. Ground data modeling - L-MEB

The in-situ soil moisture measurements are input to the L-band Microwave Emission of the Biosphere (L-MEB) model [9] to simulate brightness temperatures using auxiliary data on soil properties (i.e. soil texture, bulk density, roughness), climate and vegetation conditions. L-MEB is built for uniform scenes with certain model characteristics and calibration parameters. In this study an L-MEB version along the lines of the SMOS soil moisture (L2) processor

(referred to 'breadboards' hereafter) is used [10]. To account for mixed land cover pixels observed at large spatial scales in the breadboards different generic forward model versions with specific sets of default parameters exist for different land cover types.

1) Theory: L-MEB is based on a simplified (zero-order) radiative transfer equation [45]–[47] representing the soil as flat surface in contact with the atmosphere, and the vegetation as a homogeneous layer. According to the Rayleigh-Jeans Law in the microwave domain of the electromagnetic spectrum the radiation as measured by a radiometer is directly proportional to brightness temperature T_B. Brightness temperature depends on incidence angle θ and polarization p (H or V) and is directly related to the physical temperature T and the emissivity e/reflectivity Γ as following:

$$T_B(\theta, p) = e_{\theta,p} \cdot T$$
$$with \;\; \Gamma = 1 - e \tag{1}$$

As the received signal originates from various sources, the total brightness temperature is a composite of the following terms: 1) the soil emission attenuated (scattered and absorbed) by the canopy layer, 2) the direct canopy emission, 3) the canopy emission reflected by the soil and again attenuated by the canopy, 4) the direct sky emission and 5) the sky emission reflected by the soil and twice attenuated by the canopy layer.

In L-MEB the sky contribution to the brightness temperature is calculated according to [48], while the effects of soil and vegetation on the brightness temperature are described by the so called '$\tau - \omega$ model' [49]:

$$T_B(\theta, p) = (1 - \omega_{\theta,p})(1 - \gamma_{\theta,p})(1 + \Gamma_{\theta,p}\gamma_{\theta,p})T_v + (1 - \Gamma_{\theta,p})\gamma_{\theta,p}T_{EFF} \tag{2}$$

ω is the single scattering albedo of the canopy, γ describes the vegetation transmissivity, and T_v and T_{EFF} denote vegetation and soil effective temperature, respectively.

The vegetation transmissivity γ is calculated from the vegetation optical depth at nadir τ_{NAD} as following:

$$\gamma(\theta, p) = \exp(\tau_{NAD}/\cos\theta) \tag{3}$$

τ_{NAD} increases with increasing vegetation water content, consequently reducing the transmission of the soil brightness temperature through the vegetation. Depending on the available data L-MEB assumes a linear relationship between the optical depth at nadir, and either the vegetation water content (WVC) as developed by [50] or the leaf area index (LAI):

$$\tau_{NAD} = b \cdot VWC \tag{4}$$

$$\tau_{NAD} = b'LAI + b'' \tag{5}$$

The vegetation parameters b', b'' and b are mainly a function of canopy type/structure. In case of b a dependency on sensor frequency, polarization and incidence angle has also been noted.

To account for effects of a dominant vertical vegetation structure on the optical depth, a parameterization has been developed that expresses the nadir-equivalent optical depth as function of both incidence angle and polarization by means of the parameters tt_H and tt_V, respectively.

T_{EFF} is computed from the soil surface temperature (approximately 0-5 cm depth interval) and the deep soil temperature (approximately at 50 cm) with varying contributions as a function of soil moisture according to the formulation developed by [51] based on [52].

The roughness of a soil surface influences its reflectivity. Based on a gradually adjusted semi-empirical approach originally developed by [53], [54] and modified by [55] in L-MEB the reflectivity of a naturally occurring more or less rough surface Γ is related to the reflectivity of a perfectly flat surface (fresnel reflectivity) Γ^*. The Fresnel reflectivity is then linked to the dielectric properties of the soil through the Fresnel equations, which in turn are related to soil moisture by means of soil property information (e.g. sand and clay fractions, soil bulk density) and the Dobson dielectric mixing model [56] using the Peplinski formulation [57], [58]. The roughness correction of the reflectivity term is given by the following equation:

$$\Gamma(\theta,p) = [(1 - Q_R(\theta,p))\Gamma^*(\theta,p) + Q_R(\theta,p)\Gamma^*(\theta,p)] \exp[-H_R(\theta,p)\cos^{N_R}(\theta,p)] \quad (6)$$

Γ^*, H_R, Q_R, and N_R all depend on incidence angle and polarization. H_R describes the intensity of the roughness effects (soil reflectivity decreases as H_R increases), Q_R represents the polarization mixing effects (the difference between the reflectivity of the H and V polarizations decreases as Q_R increases), and N_R allows the modulation of the reflectivity as a function of the incidence angle. [59] showed that for the latter coefficients should be distinguished for the two polarizations (i.e. N_{RH} and N_{RV}) which also led to improved results in [9].

Roughness is primarily understood as a geometric effect in relation with spatial variations in the soil surface height. As many studies also reported an H_R-dependence on soil moisture (e.g. [27], [51], [59]–[63]) in the breadboards the roughness parameter is implemented as a piecewise function of soil moisture with constant values below a transition moisture value (defining H_R) and above field capacity (defining H_{R_Min}), while it is linearly decreasing between the two (soil texture-dependent) points.

Several H_R-parameterizations based on relationships with either the standard deviation of the surface height S_D, the correlation length L_C, or both have been developed [51], [53], [60], [64] for potential future build-in into L-MEB. The most recent nonlinear H_R-S_D relation based on a dataset covering the entire range of surface roughness conditions that can be expected on agricultural fields (S_D 4.57-59.37 mm) is as follows [64]:

$$H_R = (0.9437 S_D/(0.8865 S_D + 2.2913))^6 \quad (7)$$

Besides the soil characteristics (i.e. soil texture and soil bulk density), the choice of the vegetation parameters b/τ_{NAD} and the roughness parameter H_R have most impact on the resulting modelled brightness temperature. Especially the high importance of the latter is frequently mentioned in literature (e.g. [23], [25], [26], [29]).

2) Choice of parameter settings and related uncertainties: In this study brightness temperatures were modeled at 0 and 40° θ for each campaign ground sampling point per patch and date with individually adjusted model parameter settings as a function of inherent land cover conditions. By means of the land cover information recorded for each sampling point per patch and date, all points were allocated into the land cover classes listed in Table III. The nominal generic forward model for low vegetation ('FNO') was applied for all classes except for 'coniferous forest' and 'trees' where the forest model ('FFO') was used. The respective default parameter settings were adjusted wherever findings from recent studies or field measurements for the parameterization were available. For the most important input parameters (soil moisture, bulk density, texture, H_R and τ_{NAD}) a range of possible values was defined in order to study model uncertainty.

The average, maximum and minimum (+/- one standard deviation) of the 3 calibrated mineral soil moisture probe readings were calculated at each location for model input.

For the estimation of the effective soil temperature T_{EFF} surface (0-5 cm) and deep soil temperatures (50-55 cm depth) recorded at the time of the soil moisture sampling were extracted from soil moisture network stations situated within each of the three respective patches. Air temperature and pressure data at 2 m height with coincident time stamps were taken from the four closest DMI climate stations. Canopy temperature T_V was approximated by either 2 m air or 0-5 cm soil temperature in case of the presence of tall vegetation (classes 'coniferous forest' and 'trees') or low vegetation, respectively.

Different texture scenarios (average % Sand/average % Clay, minimum % Sand/maximum % Clay, maximum % Sand/minimum % Clay) from both the Danish Soil Grid [40] and the site-specific texture analysis of the campaign samples (HOBE texture data) were applied.

For sampling locations where a gravimetric soil sample was taken dry soil bulk density was calculated from the latter while in all other cases the average per patch and sampling date was applied. For the uncertainty study maximum and minimum values were estimated by means of +/- one standard deviation. The solid particle density was set to the constant default value of 2.664 g/cm^3.

At L-band scattering effects are generally low. In all model runs the scattering albedo ω was set to the default values 0 and 0.08 for low vegetation and forest, respectively, according to e.g. [23], [25]. As the dependence of the scattering albedo on incidence angle and polarization could not yet been clearly demonstrated the diff_ω-term was set to 0 in all cases.

Value ranges and most likely 'uni' values for τ_{NAD} are compiled in Table III. In case of the forest land cover classes they were directly defined based on [24], [25], [65]. For the other land cover classes where vegetation water content measurements were available, using Eq. (4) a range of τ_{NAD} values was calculated by means of corresponding ranges of VWC and b values, while a most likely 'uni' τ_{NAD} value was estimated by the respective average VWC and 'uni' b values. The VWC data was linearly interpolated between the two sampling dates to obtain a value range (avg. and min/max from interpolated standard deviation) for each of the four flight dates. In case of agriculture grass an average of the two available samples was taken. For b the ranges of possible values including a most likely value 'uni' were defined based on various literature [9], [26]–[28], [50], [62], [66]–[68] (Table III).

For crops most values were reported to lie between 0.8 (SMOS L2 default) and 0.15. 0.11 was selected as most likely value 'uni' along the lines of [68]. In case of native grass (with litter) the interval was chosen between 0.1 and 0.3 with 0.12 (SMOS L2 default) as 'uni'-value. For the not regularly cut agricultural grass and for heather where no specifications were found in literature the same values as for native grass were applied.

Assuming polarization and incidence angle independence of the optical depth, tt_H and tt_V were both set to 1 throughout this study.

Q_R was set to 0 throughout this study in accordance with the findings of various studies (e.g. [51], [60], [64], [69], [70]).

The behavior of N_{RH} and N_{RV} is currently not well understood as no clear relation between the two parameters has yet been found. Generally, it has been stated that they lie between -2 and 2 and N_{RH} is larger than N_{RV} except for surfaces covered with plants of dominant vertical structure [25]. In agreement with previous studies [64] discovered a difference (N_{RH}-N_{RV}) in the order of 2 for smooth fields. In this study the two combinations N_{RH}=2 and $N_{RV} = 0$ (SMOS L2 default) and N_{RH}=0 and N_{RV}=-1 (e.g. [9], [26]) were tested in order to span the range of reasonable assumptions based on literature findings.

In this study the soil moisture-dependent parametrization of H_R was neglected (i.e. H_R=H_{R_Min}) as it remains controversial [71]. For landcover classes where surface roughness measurements were available as well as for classes of similar appearance in terms of roughness, using Eq. (7) a most likely H_R value 'uni' and a min-max range were calculated by means of the average and max/min (+/-1 standard deviation) S_D, respectively (Table III). For the heath classes 'natural grass', 'scotch heather', and 'scotch heather/grass' a value range of 0.5-1.1 with a 'uni' value 0.8 was chosen in accordance with the retrieval results of [26], [28], [29], [62] as well as the SMOS L2 default. In case of the forest classes we adapted the findings of [25], i.e. 1.0-1.2 with 'uni' value 1.1.

3) Data modeling and scaling: Using these defined parameter settings brightness temperatures were modeled for different scenarios. Additionally to a model run with all parameters set to their respective 'uni'/average values, runs were conducted by means of all possible combinations of minimum and maximum values of the parameters with highest impact on the model result, namely soil moisture, soil bulk density, soil texture, H_R and τ_{NAD}. First, the N_{RH} and N_{RV} were set to 2 and 0, respectively, (SMOS L2 default), then this analysis was repeated with N_{RH}=0 and N_{RV}=-1. With respect to soil texture, the minimum-maximum range is defined on the basis of the site-specific texture analysis. The effect of applying site-specific soil texture data instead of soil texture information extracted from the Danish topsoil grid was investigated in a separate model run.

To obtain values comparable to the airborne brightness temperatures, the modeled brightness temperatures from each model run were averaged per respective sampling patch and date. In addition to the simple average a weighted average was generated by allocating a weight based on the EMIRAD-2 antenna pattern as described in [38] to each ground sampling point's data. Likewise, for comparison with SMOS data all EMIRAD measurements acquired over the SMOS pixel were averaged per sampling day by (1) a simple mean, and (2) a weighted mean taking the average SMOS antenna pattern into account [10](Fig. 1a).

IV. Results and Discussion

A. Model input parameters

The soil moisture data compiled in Table I reveals a high spatial variability within all sampling patches, but no considerable changes in average moisture content were observed between the different campaign sampling days as a result of only few insignificant rain events (below 3 mm in each case) during the 2-weeks campaign window. Throughout the campaign, driest conditions were found in the agriculture patch with a more pronounced precipitation-moisture response. In case of heath and forest the latter is dampened by the presence of the moss/organic layers.

The parameters estimated based on actual field data (Table III) were compared with literature findings to judge their reliability. Generally, the computed optical depths seem to agree well with values found in literature for similar plant types and vegetation water contents at this time of the year (see e.g. [9], [50], [68]). For example the optical depth of 0.08 for winter rye with b and VWC of 0.114 and 0.7 kg/m^2, respectively, as listed in [50], fits very well with the estimated winter barley data. A τ_{NAD} of 0.1 as retrieved by [29] for mediterranean bushland is within the range of the scotch heather values. For grass the VWC-τ_{NAD} relations stated in [50] and [61] (i.e. ca VWC 0.2-0.8 kg/m^2 and τ_{NAD} 0.1-0.3) match our maximum τ_{NAD} values very well, while the ones described by [62] for alfalfa and seeded clover grass without litter (i.e. approximately VWC 0.5-1.3 kg/m^2 and τ_{NAD} 0.04-0.11) are in better agreement with out 'uni' τ_{NAD} values.

The estimated S_D values span the entire interval of roughness conditions expected on agricultural fields and seem to be in same magnitude as numbers reported from other experiments (e.g. [23], [72]). The resulting H_R values are higher than the SMOS L2 default for crops (0.2) which is in good agreement with recent studies by [26]–[28] who suggested that the latter was too low. However, our H_Rs are still in a lower order than the ones found by these authors in their retrieval analysis. In contrast, in case of the heath classes the literature values for natural grass and shrubs indicate a higher probability of H_R in the lower end of the chosen range. The forest surfaces including clearings are of very rough appearance which should justify the constantly high chosen H_Rs.

B. Comparison ground - airborne data

Fig. 4 shows the results of the modeled brightness temperatures from the 'average-run' and the runs using all possible combinations of minimum/maximum values for the 5 selected parameters with N_{RH}=2/0 and N_{RV}=0/-1 for all patch types, sampling dates, H and V polarizations, and 0 and 40° incidence angles, respectively. As expected the behavior of soil moisture is reproduced in the modeling results as well as in the EMIRAD data. The measured brightness temperatures lie in a very narrow interval reflecting the aforementioned small temporal variability of prevailing soil moisture conditions. Also, the stronger precipitation-moisture response on the agricultural site without the presence of a dampening organic layer can be recognized in the figures despite of the lack of distinct rain events during the studied period. Particularly striking are the vast range of modeled brightness temperatures (in the order of 40 - 60 K) resulting from the different model runs as well as the clear tendency of the model to underestimate

the EMIRAD-2 data. Both features are observable in constant manner throughout all patch types, sampling dates, polarizations and incidence angles, being least pronounced for the 40° V-polarization while strongest in the 40° H-polarization. Nevertheless, under certain constellations of input parameters the modeled ground data can be brought into agreement with the EMIRAD-2 data throughout all sampling patches, campaign dates, for both polarizations and incidence angles, respectively. To our believe input parameters have been chosen within reasonable ranges. In the following optimum parameter constellations will be analyzed with respect to the role of individual parameters.

Table IV shows the mean RMSE values for the individual patch and radiometer configurations as well as for the combination of all configurations averaged over all model runs for N_{RH}=2/0 and N_{RV}=0/-1, respectively. While the RMSE averaged over all patches remains unchanged in the nadir configurations between the N_{RH}=2/0 and N_{RV}=0/-1 scenarios it becomes apparent that it improves significantly in the 40° H-polarization from 34.49 K for N_{RH}=2/N_{RV}=0 to 22.52 K for N_{RH}=0/N_{RV}=-1. The enhanced model performance can also be traced in the 40° V-polarization averaged over all patch types and in the overall RMSE, though to a smaller extent, with ameliorations from 10.49/19.93 K for N_{RH}=2/N_{RV}=0 to 8.5/16.46 K for N_{RH}=0/N_{RV}=-1, respectively. This is in agreement with a previously conducted L-MEB sensitivity study with our data (not shown) confirming that choosing different combinations of N_{RH} and N_{RV} within the -2 to 2 range only influenced the modeled brightness temperatures at the 40° incidence angle and more in H- than V-polarization. Furthermore, these findings are in accordance with the statement by [64] that the N_R parameter may have strong impact on the emissivity at large incidence angles as well as a with a recent study by [73]. The latter found an inverse relationship between standard deviation of heights and N_R according to which the choice of lower N_R values for our sites with a general tendency to rather rough surface conditions seems reasonable.

Table V specifies the 7 best-fit model runs ranked after RMSE values averaged over all patch and radiometer configurations, the 'average'-run as reference and the overall average of all runs, patch types, and radiometer configurations, for N_{RH}=2/N_{RV}=0 and N_{RH}=0/N_{RV}=-1, respectively. In comparison with the 'average'-run RMSE values are significantly smaller for the highest ranked best-fit runs. The ranking which is based on the overall average RMSE also remains fairly stable throughout the individual patch type/radiometer configurations (not shown). While the best-fit ranking of the two N_R scenarios are consistent, again in all cases the RMSE values of the N_{RH}=0/N_{RV}=-1 model runs are lower than the ones of the N_{RH}=2/N_{RV}=0 runs. Also the standard deviations are markedly lowered which is mainly caused by significant differences in the RMSEs in the 40° H-polarization. These are further indications that the N_{RH}=0/N_{RV}=-1 scenario apparently shows a better overall performance.

Table V also reveals that in case of all seven 'best-fit' model runs the H_R is constantly set to the maximum value and the texture scenario to minimum fraction of sand/maximum fraction of clay. As stated above in case of the agriculture classes high H_Rs are concordant with literature findings which even suggest higher values than the ones used in this study. In fact, increasing the roughness parameter in our case would counteract the tendency of underestimating EMIRAD T_Bs.

To study the effect of applying site-specific soil texture data instead of soil texture information extracted from the Danish topsoil grid, two separate model runs were conducted with either of the two texture data (average fractions

of sand and clay) and in both cases maximum H_R and τ_{NAD}, average soil moisture, dry bulk density as estimated at individual locations or patch average, and N_{RH}=0/N_{RV}=-1. The results are shown in Fig. 5. For all radiometer configurations, the RMSE of the agriculture site improves significantly by using the site-specific soil texture data, while for the heath and forest patches there is only a slight deterioration towards somewhat higher RMSE values. This is consistent with the finding of constant minimum sand/maximum clay fractions in the 'best-fit' model runs as sand/clay fractions are lower/higher in the HOBE texture data compared to the ones suggested by the Danish soil grid, and thus shows the benefit of acquiring site-specific texture information for such validation activities instead of using data with a coarse spatial resolution.

Generally, the fit between modeled and measured brightness temperatures is best in case of the forest site while for the agriculture site we find largest deviations from the 1:1 line. Indeed we would expect the opposite since we can assume that in case of the agriculture site the data and model parameters correspond best to true conditions resulting in most reliable model results due to the following reasons: (1) most accurate sensor- and site-specific Theta sensor calibration due to less spatial variability in the underlying data, denser sampling spacing with significantly more data points and one additional sampling day, (3) some of the most important model parameters (vegetation, roughness) are directly computed by means of field measurements while in case of forest and heath land covers even literature values were much sparser or at all unavailable (e.g. for scotch heather), (4) presence of much more pronounced vegetation layers at the heath and especially forest site that certainly superimpose the soil moisture signal captured by the radiometer, plus also (5) presence of distinct layers of moss and organic material on top of the mineral soil (around 5-20 cm in thickness) exhibiting much higher water contents and thus dampening the precipitation-moisture response in the mineral soil at these sites [36]. Recalling that the signal penetration depth at L-band is < 5 cm for very wet soils implies that with maximum likelihood emissions measured by the radiometer originate solely from these very wet overlying layers. This suggests that our model runs are driven by too low soil moisture input which in turn should then result in too high modeled brightness temperatures compared to the EMIRAD-2 data. As this is not the case, and we are still obtaining a very good fit for some of the model runs, certain model parameters are compensating for the bias resulting from these not considered effects. It might stand to reason to assume that H_R and b/τ_{NAD} are set too high - at least in case of the roughness parameter this is in agreement with literature findings pointing to rather lower values. It will be of high interest in the future to investigate this further by taking the moss/organic layer data into account and not only run L-MEB in forward mode, but retrieve parameters using the knowledge gained so far to constrain the model.

Finally, to investigate the impact of a simple versus a weighted mean (taking the EMIRAD-2 antenna pattern into account) the output of the model run from the texture study using the HOBE texture was averaged by means of both methods (per respective sampling patch and date). Results show that for all radiometer configurations there is no significant change between the two. (Fig. 6).

C. Comparison airborne - spaceborne data

Fig. 7 depicts EMIRAD-2 brightness temperatures recorded over all ten flight tracks within the Danish validation site as well as the SMOS L1C TOA (ascending overpass) data of the corresponding SMOS node 2002029 over all observed incidence angles and for H and V polarization, respectively, on the only RFI-free sampling day, May 02. Due to artefacts in the instrument's measurement configuration the SMOS data is deviating from the ideal Fresnel curve expected over a land surface. This is especially pronounced in the low incidence angles acquired in the only near alias-free part of the SMOS field of view. Even though alias effects are corrected and damaged measurements filtered there are currently some remaining disturbances in the data. With respect to the EMIRAD data the scatter in the measured brightness temperatures in the order of 20 K in both polarizations and incidence angles stands out. It reflects the encountered spatial variability of land surface conditions within the observed SMOS pixel.

Generally, the two datasets agree well with a slight positive bias of the airborne data. To facilitate comparison a second order polynomial curve has been fitted through the SMOS data. RMSE values calculated on the basis of this 'Fresnel curve' are 7.74, 8.30 and 9.33 and 5.58 K for 0° H, V and 40° H, V incidence angles, respectively, though the comparison at nadir has to be taken with care as the SMOS data is extrapolated at this point. [74] found that for a heterogeneous land surface typically a minimum of 50% airborne data coverage of the SMOS pixel were required for an expected sampling error of less than 4 K, the design sensitivity of SMOS. In our case, 35% of the SMOS pixel could be covered with EMIRAD data which might explain these slightly higher deviations. As in case of the modeled ground data, the application of the weighted average by means of the SMOS antenna pattern did not alter the results for any of the polarizations and incidence angles on all 4 sampling dates (Table VI). Evidently, no sound conclusions about the goodness of SMOS data for this area can be drawn from this single-day comparison. Nevertheless, this result is a promising start for further investigations that are planned in the near future. By means of the continuous measurements of the soil moisture network installed in the Skjern River Catchment the temporal constraints of the airborne validation campaign can be overcome.

V. Conclusions and Outlook

An airborne SMOS Cal/Val campaign with the passive L-band radiometer EMIRAD-2 and simultaneous soil moisture ground sampling was carried out in the Skjern River Catchment, Denmark, within the framework of HOBE. This study presents the step-wise validation approach over spatial scales from point (ground data) to intermediate (EMIRAD-2) to large (SMOS) scale by means of the campaign dataset.

Comparisons were carried out at brightness temperature level at the top of the atmosphere (SMOS L1C data, HV). In case of the ground measurements the L-MEB forward model was used to model brightness temperatures from the soil moisture data with parameter choice based on thorough literature review as well as parameterization using campaign field measurements. The influence of parameter uncertainty on the resulting brightness temperatures was investigated and with respect to upscaling the modeled point data to the airborne scale and the airborne data to SMOS scale the datasets were averaged by means of a simple and a weighted mean taking the EMIRAD and SMOS antenna patterns into account, respectively.

Estimated parameter uncertainties result in a considerable range of modeled brightness temperatures. Nevertheless, under certain constellations of input parameters our modeled ground data agrees with the EMIRAD data on all sampling patches, campaign dates, for both polarizations and incidence angles, respectively. Analyzing the best-fit parameter combinations shows that the use of site-specific texture information improves the fit compared to using soil texture information from a grid with coarse spatial resolution. Likewise, the choice of a lower set of N_R values increases the overall agreement between modeled and measured brightness temperatures compared to using the SMOS default settings of this parameter. Furthermore, a high probability that the H_R should be set close to the maximum of the chosen range is suggested.

We conclude, that the method of adjusting model parameter settings for each individual sampling point based on inherent land cover conditions seems to hold well, and so does the adaption of parameter values from other studies. However, although we are able to point out tendencies towards maximum likelihood parameter estimates a considerable uncertainty remains. With the applied forward approach an isolated view on individual components is challenging. To constrain the uncertainty of individual model parameters in the future will necessitate a combination of our approach with retrieval studies.

This will be of particular interest for land cover types where currently literature data is sparse or not available at all, as in our case for the heath and forest land covers. With respect to the latter only data from the mineral soils was considered in this study. However, significantly wetter moss and organic layers of considerable thickness are present on top of the mineral soils implying that the signal measured by the radiometer is at with highest probability originating there from. Thus, the good agreement between modeled brightness temperatures with soil moisture input from the underlying much drier mineral soils and the EMIRAD-2 data can solely result from certain model parameters compensating for the bias. This issue remains to be tackled in the future by means of parameter retrieval approaches and using the knowledge gained so far to constrain the model.

This study gives evidence for the suitability of a step-wise SMOS validation approach. Beside the ability to reproduce EMIRAD-2 measurements by means of modeled brightness temperatures, we can similarly claim that EMIRAD-2 and SMOS data show good accordance on the single day where comparison was not prevented by strong RFI. Thereby, applying weights based on the radiometer antenna pattern did not affect the resulting brightness temperatures neither in case of modeled ground data nor EMIRAD-2. It is evident that no final statement on the goodness of SMOS over the Danish Cal/Val site can be drawn at this point. Apart from the drawback of a limited dataset due to RFI issues, our data validation is also restricted in terms of a narrow brightness temperature interval which reflects the small temporal variability of prevailing soil moisture conditions throughout the 2-weeks campaign window. Further SMOS validation work carried out over longer time frames and additional at soil moisture level (SMOS L2 data) is currently performed by means of the soil moisture network data especially designed for that purpose. Thereby, the gained knowledge from the campaign data will be of great value. Once the confidence on the goodness of SMOS data at the studied grid node will be deepend, the validation activities will also be expanded to the surrounding SMOS grid nodes with higher open water fractions to study the impact of the latter on the SMOS soil moisture data quality.

ACKNOWLEDGMENT

The project is funded by the Villum Kann Rasmussen Foundation and the Technical University of Denmark. Special thank goes to the HOBE members involved in the organization of the airborne campaign and the motivated ground sampling teams who did an excellent job. Furthermore, the authors would like to thank the SMOS team at CESBIO for valuable discussions and providing codes for modeling and data processing. We were also very thankful for the ThetaProbes supplied by CESBIO and AALTO University.

REFERENCES

[1] J. S. Famiglietti, J. W. Rudnicki, and M. Rodell, "Variability in surface moisture content along a hillslope transect: Rattlesnake hill, texas," *Journal of Hydrology*, vol. 210, pp. 259–281, 1998.

[2] B. P. Mohanty, T. H. Skaggs, and J. S. Famiglietti, "Analysis and mapping of field-scale soil moisture variability using high-resolution, ground-based data during the southern great plains 1997 (sgp97) hydrology experiment," *Water Resources Research*, vol. 36, no. 4, pp. 1023–1031, 2000.

[3] A. W. Western, R. B. Grayson, and G. Bloeschl, "Scaling of soil moisture: a hydrologic perspective," *Annual Review of Earth and Planetary Sciences*, vol. 30, pp. 149–180, 2002.

[4] Y. Kerr, P. Waldteufel, J.-P. Wigneron, J.-M. Martinuzzi, J. Font, and M. Berger, "Soil moisture retrieval from space: The soil moisture and ocean salinity (smos) mission," *IEEE Transactions on Geoscience and Remote Sensing*, vol. 39, no. 8, 2001.

[5] Y. Kerr, "Soil moisture from space: Where are we?" *Hydrogeology Journal*, vol. 15, pp. 117–120, 2007.

[6] W. Wagner, G. Blöschl, P. Pampaloni, J.-C. Calvet, B. Bizzarri, J.-P. Wigneron, and Y. Kerr, "Operational readiness of microwave remote sensing of soil moisture for hydrologic applications," *Nordic Hydrology*, vol. 38, no. 1, pp. 1–20, 2007.

[7] S. Raju, A. Chanzy, J.-P. Wigneron, J.-C. Calvet, Y. Kerr, and L. Laguerre, "Soil moisture and temperature profile effects on microwave emission at low frequencies," *Remote Sensing of Enviornment*, vol. 54, no. 2, pp. 85–97, 1995.

[8] C. Laymon, W. Crosson, T. Jackson, A. Manu, and T. Tsegaye, "Ground-based passive microwave remote sensing observations of soil moisture at s-band and l-band with insight into measurement accuracy," *IEEE Transactions on Geoscience and Remote Sensing*, vol. 39, pp. 1844–1858, 2001.

[9] J.-P. Wigneron, Y. Kerr, P. Waldteufel, K. Saleh, Escorihuela, M.-J., P. Richaume, P. Ferrazzoli, P. de Rosnay, R. Gurney, J.-C. Calvet, J. Grant, M. Guglielmetti, B. Hornbuckle, C. Mätzler, T. Pellarin, and M. Schwank, "L-band microwave emission of the biosphere (l-meb) model: Description and calibration against experimental data sets over crop fields," *Remote Sensing of Environment*, vol. 107, pp. 639–655, 2007.

[10] Y. Kerr, P. Waldteufel, P. Richaume, P. Davenport, P. Ferrazzoli, and J.-P. Wigneron, "Smos level 2 processor soil moisture algorithm theoretical basis document (atbd)," CBSA, UoR, TV and INRA, Toulouse, Tech. Rep. SO-TN-ARR-L2PP-0037, V3.4, 24/01/2011 2011.

[11] E. Daganzo, J. Pla, Y. Kerr, M. Martin-Neira, R. Oliva, E. Marelli, S. Mecklenburg, B. Rommen, M. Brown, P. Richaume, and C. Gruhier, "Characterisation of smos rf interferences in the 1400-1427 mhz band as detected during the commissioning phase," in *OCOSS 2010*, Brest, France, 2010.

[12] N. Skou, S. Misra, J. E. Balling, S. S. Kristensen, and S. S. Søbjærg, "L-band rfi as experienced during airborne campaigns in preparation for smos," *IEEE Transactions on Geoscience and Remote Sensing*, vol. 48, no. 3, pp. 1398–1407, March 2010b.

[13] N. Skou, J. Balling, S. S. Søbjærg, and S. S. Kristensen, "Surveys and analysis of rfi in the smos context," in *Proceedings of IGARSS*, July 2010c, pp. 2011–2014.

[14] A. Camps, J. Gourrion, J. M. Tarongi, A. Gutiérrez, and R. Castro, "Rfi analysis in smos imagery," in *Proceedings of IGARSS*, July 2010, pp. 2007–2010.

[15] S. Delwart, C. Bouzinac, P. Wursteisen, M. Berger, M. Drinkwater, M. Martin-Neira, and H. Kerr, Yann, "Smos validation and the cosmos campaign," *IEEE Transactions on Geoscience and Remote Sensing*, vol. 46, no. 3, pp. 695–704, 2008.

[16] M. Cosh, T. Jackson, R. Bindlish, and J. H. Prueger, "Watershed scale temporal and spatial stability of soil moisture and its role in validating satellite estimates," *Remote Sensing of Environment*, vol. 92, pp. 427–435, 2004.

[17] T. Jackson, T. Schmugge, and P. O'Neill, "Passive microwave remote sensing of soil moisture from an aircraft platform," *Remote Sensing of Enviornment*, vol. 14, pp. 135–151, 1984.

[18] T. Schmugge, J. Wang, and G. Asrar, "Results from the push broom microwave radiometer flights over the konza prairie in 1985," *IEEE Transactions on Geoscience and Remote Sensing*, vol. 26, no. 5, 1988.

[19] T. Jackson, D. Le Vine, A. Hsu, A. Oldak, P. Starks, C. Swift, J. Isham, and M. Haken, "Soil moisture mapping at regional scales using microwave radiometry: The southern great plains hydrology experiment," *IEEE Transactions on Geoscience and Remote Sensing*, vol. 37, no. 5, 1999.

[20] R. Bindlish, T. Jackson, A. Gasiewski, B. Stankov, M. Klein, M. Cosh, I. Mladenova, C. Watts, E. Vivoni, V. Lakshmi, J. Bolten, and T. Keefer, "Aircraft based soil moisture retrievals under mixed vegetation and topographic conditions," *Remote Sensing of Environment*, vol. 112, pp. 375–390, 2008.

[21] R. Panciera, J. Walker, J. Kalma, E. Kim, J. Hacker, O. Merlin, M. Berger, and N. Skou, "The nafe'05/cosmos data set: Toward smos soil moisture retrieval, downscaling, and assimilation," *IEEE Transactions on Geoscience and Remote Sensing*, vol. 46, no. 3, pp. 736–745, 2008.

[22] O. Merlin, J. Walker, J. Kalma, E. Kim, J. Hacker, R. Panciera, R. Young, G. Summerell, J. Hornbuckle, M. Hafeez, and T. Jackson, "The nafe'06 data set: Towards soil moisture retrieval at intermediate resolution," *Advances in Water Resources Research*, vol. 31, pp. 1444–1455, 2008b.

[23] M. Pardé, J.-P. Wigneron, P. Waldteufel, Y. Kerr, A. Chanzy, S. S. Søbjærg, and N. Skou, "N-parameter retrievals from l-band microwave observations acquired over a variety of crop fields," *IEEE Transactions on Geoscience and Remote Sensing*, vol. 42, no. 6, pp. 1168–1178, June 2004.

[24] J. Grant, J.-P. Wigneron, A. Van de Griend, A. Kruszewski, S. Schmidl Søbjærg, and N. Skou, "A field experiment on microwave forest radiometry: L-band signal behavior for varying conditions of surface wetness," *Remote Sensing of Environment*, vol. 109, pp. 10–19, 2007.

[25] J. Grant, K. Saleh-Contell, J.-P. Wigneron, M. Guglielmetti, Y. Kerr, M. Schwank, N. Skou, and V. de Griend A., "Calibration of the l-meb model over a coniferous and a deciduous forest," *IEEE Transactions on Geoscience and Remote Sensing*, vol. 46, no. 3, pp. 808–818, March 2008.

[26] R. Panciera, J. Walker, and O. Merlin, "Improved understanding of soil surface roughness parameterization for l-band passive microwave soil moisture retrieval," *IEEE Geoscience and Remote Sensing Letters*, vol. 6, no. 4, pp. 625–629, October 2009a.

[27] R. Panciera, J. Walker, J. Kalma, E. Kim, K. Saleh, and J.-P. Wigneron, "Evaluation of the smos l-meb passive microwave soil moisture retrieval algorithm," *Remote Sensing of Environment*, vol. 113, pp. 435–444, 2009b.

[28] K. Saleh, Y. Kerr, P. Richaume, M.-J. Escorihuela, R. Panciera, S. Delwart, G. Boulet, P. Maisongrande, J. Walker, P. Wursteisen, and J.-P. Wigneron, "Soil moisture retrievals at l-band using a two-step inversion approach (cosmos/nafe'05 experiment)," *Remote Sensing of Environment*, vol. 113, pp. 1304–1312, 2009.

[29] A. Cano, K. Saleh, J.-P. Wigneron, C. Antolín, J. E. Balling, Y. Kerr, A. Kruszewski, C. Millán-Scheiding, S. Schmidl Søbjærg, N. Skou, and E. López-Baeza, "The smos mediterranean ecosystem l-band characteristation experiment (melbex-i) over natural shrubs," *Remote Sensing of Environment*, vol. 114, pp. 844–853, 2010.

[30] S. Peischl, J. P. Walker, C. Rudiger, Y. Nan, Y. Kerr, and E. Kim, "The aaces field experiments: Smos calibration and validation across the murrumbidgee river catchment," *Transactions on Geoscience and Remote Sensing*, vol. This Issue, In Review.

[31] J. T. Dall'Amico, F. Schlenz, A. Loew, and W. Mauser, "Smos soil moisture validation: Status at the upper danube cal/val site eight monghts after launch," in *IEEE International Geoscience and Remote Sensing Symposium (IGARSS)*, Honolulu, Hawaii, USA, 2010, pp. 3801–3804.

[32] J. T. Dall'Amico, F. Schlenz, A. Loew, W. Mauser, J. Kainulainen, J. E. Balling, and C. Bouzinac, "Airborne and ground campaigns in the upper danube catchment: Data sets for calibration, validation and downscaling of smos data," *IEEE Transactions on Geoscience and Remote Sensing*, In Review.

[33] J. Kainulainen, K. Rautiainen, P. Sievinen, J. Seppa?nen, E. Rouhe, M. Hallikainen, J. Dall'Amico, F. Schlenz, A. Loew, S. Bircher, and C. Montzka, "Smos calibration and validation activities with airborne interferometric radiometer hut-2d during spring 2010," in *Geoscience and Remote Sensing Symposium (IGARSS)*, Honolulu, HI, USA, 25-30 July 2010, pp. 702–705.

[34] C. Albergel, E. Zakharova, J.-C. Calvet, M. Zribi, M. Pardé, J.-P. Wigneron, N. Novello, Y. Kerr, A. Mialon, and N. Fritz, "A first

assessment of the smos data in southwestern france using in situ and airborne soil moisture estimates: the carols airborne campaign," *Transactions on Geoscience and Remote Sensing*, vol. This Issue, In Review.

[35] A. Kontu, J. Lemmetyinen, J. Pulliainen, K. Rautiainen, J. Kainulainen, and J. Seppa?nen, "L-band measurements of boreal soil," in *IEEE International Geoscience and Remote Sensing Symposium (IGARSS)*, no. Digital Object Identifier: 10.1109/IGARSS.2010.5654116, 2010, pp. 706–709.

[36] S. Bircher, J. Balling, and N. Skou, "Smos validation activities at different scales in the skjern river catchment, western dk," in *ESA Living Planet Symposium*, H. Lacoste-Francis, Ed., ESA. Bergen, Norway: ESA communications, 28. June - 02. July 2010.

[37] N. Skou, S. Søbjærg, J. Balling, and S. Kristensen, "A second generation l-band digital radiometer for sea salinity campaigns," in *Geoscience and Remote Sensing Symposium (IGARSS)*, Denver, CO, USA, 31. July - 04. August 2006, pp. 3984–3987.

[38] N. Skou, S. S. Søbjærg, J. Balling, S. S. Kristensen, and A. Kusk, "Emirad-2 and its use in the smos cal/val campaign," DTU Space, Kgs. Lyngby, Denmark, Tech. Rep. AR 502, June 2010a.

[39] J. Cappelen, "Danmarks klima 2008 med tórshavn, færøerne og nuuk, grønland - with english translations," Danmarks Meteorologiske Institut, København, Teknisk rapport 09-01, 2009.

[40] M. H. Greve, M. B. Greve, P. Bøcher, T. Balstrøm, H. Breuning-Madsen, and L. Krogh, "Generating a danish raster-based topsoil property map combining choropleth maps and point information," *Danish Journal of Geography*, vol. 107, no. 2, pp. 1–12, 2007.

[41] K. Jensen and T. Illangasekare, "Hobe: A hydrological observatory," *Vadose Zone Journal*, vol. 10, pp. 1–7, 2011.

[42] S. Bircher, N. Skou, K. Jensen, J. Walker, and L. Rasmussen, "A soil moisture network for smos validation in the skjern river catchment, western denmark," *Vadose Zone Journal*, in prep.

[43] C. S. Ruf, S. M. Gross, and S. Misra, "Rfi detection and mitigation for microwave radiometry with an agile digital detector," *IEEE Transactions on Geoscience and Remote Sensing*, vol. 44, no. 3, pp. 694–706, March 2006.

[44] A. Jarvis, H. Reuter, A. Nelson, and E. Guevara. (2008, 26.06.2009) Hole-filled seamless srtm. data V4. International Centre for Tropical Agriculture (CIAT). [Online]. Available: http://srtm.csi.cgiar.org

[45] J.-P. Wigneron, A. Chanzy, J.-C. Calvet, and N. Bruguier, "A simple algorithm to retrieve soil moisture and vegetation biomass using passive microwave measurements over crop fields," *Remote Sensing of the Environment*, vol. 51, pp. 331–341, 1995.

[46] T. Jackson and D. Le Vine, "Mapping surface soil moisture using an aircraft-based passive microwave instrument: algorithm and example," *Journal of Hydrology*, vol. 184, pp. 85–99, 1996.

[47] E. Njoku, W. Wilson, S. Yueh, S. Dinardo, F. Li, T. Jackson, V. Lakshmi, and J. Bolten, "Observations of soil moisture using a passive and active low-frequency microwave airborne sensor during sgp99," *IEEE Transactions on Geoscience and Remote Sensing*, vol. 40, no. 12, pp. 2659–2673, 2002.

[48] T. Pellarin, J.-P. Wigneron, J.-C. Calvet, M. Berger, H. Douville, P. Ferrazzoli, Y. Kerr, E. Lopez-Baeza, J. Pulliainen, L. Simmonds, and P. Waldteufel, "Two-year global simulation of l-band brightness temperatures over land," *IEEE Transactions on Geoscience and Remote Sensing*, vol. 41, no. 9, pp. 2135–2139, September 2003.

[49] T. Mo, B. Choudhury, T. Schmugge, and T. Jackson, "A model for microwave emission from vegetation covered fields," *Journal of Geophysical Research*, vol. 11, no. 11, pp. 229–237, 1982.

[50] T. Jackson and T. . Schmugge, "Vegetation effects on the microwave emission of soils," *Remote Sensing of Environment*, vol. 36, pp. 203–212, 1991.

[51] J.-P. Wigneron, L. Laguerre, and Y. Kerr, "A simple parameterization of the l-band microwave emission from rough agricultural soils," *IEEE Transactions on Geoscience and Remote Sensing*, vol. 39, no. 8, 2001.

[52] B. Choudhury, T. Schmugger, and T. . Mo, "A parametrization of effective soil temperature for microwave emission," *Journal of Geophysical Research*, vol. 87, no. C2, pp. 1301–1304, 1982.

[53] B. Choudhury, T. Schmugge, A. Chang, and R. . Newton, "Effect of surface roughness on the microwave emission from soils," *Journal of Geophysical Research*, vol. 84, pp. 5699–5706, 1979.

[54] J. Wang and B. . Choudhury, "Remote sensing of soil moisture content over bare field at 1.4 ghz frequency," *Journal of Geophysical Research*, vol. 86, no. NC6, pp. 5277–5282, 1981, oceans and Atmospheres.

[55] C. Prigent, J.-P. Wigneron, W. Rossow, and J. Pardo-Carrion, "Frequency and angular variations of land surface microwave emissivities: Can we estimate ssm/t and amsu emissivities from ssm/i emissivities?" *IEEE Transactions on Geoscience and Remote Sensing*, vol. 38, no. 5, pp. 2372–2386, September 2000.

[56] M. Dobson, F. Ulaby, M. Hallikainen, and M. El-Reyes, "Microwave dielectric behavior of wet soil - part ii: Dielectric mixing models," *IEEE Transactions on Geoscience and Remote Sensing*, vol. 23, pp. 35–46, 1985.

[57] N. Peplinski, F. Ulaby, and M. Dobson, "Dielectric properties of soils in the 0.3-1.3-ghz range," *IEEE Transactions on Geoscience and Remote Sensing*, vol. 33, no. 3, pp. 803–807, 1995a.

[58] ——, "Corrections to 'dielectric properties of soils in the 0.3-1.3-ghz range'," *IEEE Transactions on Geoscience and Remote Sensing*, vol. 33, no. 6, p. 1340, 1995b.

[59] M. Escorihuela, Y. Kerr, P. de Rosnay, J.-P. Wigneron, J.-C. Calvet, and F. Lemaître, "A simple model of the bare soil microwave emission at l-band," *IEEE Transactions on Geoscience and Remote Sensing*, vol. 45, no. 7, pp. 1978–1987, July 2007.

[60] T. Mo and T. Schmugge, "A parameterization of the effect of surface roughness on microwave emission," *IEEE Transactions on Geoscience and Remote Sensing*, vol. GRS-25, no. 4, pp. 481–486, July 1987.

[61] K. Saleh, J.-P. Wigneron, P. de Rosnay, J.-C. Calvet, M. Escorihuela, Y. Kerr, and P. Waldteufel, "Impact of rain interception by vegetation and mulch on the l-band emission of natural grass," *Remote Sensing of Environment*, vol. 101, pp. 127–139, 2006b.

[62] K. Saleh, J.-P. Wigneron, P. Waldteufel, P. de Rosnay, M. Schwank, J.-C. Calvet, and Y. Kerr, "Estimates of surface soil moisture under grass covers using l-band radiometry," *Remote Sensing of Environment*, vol. 109, pp. 42–53, 2007.

[63] O. Merlin, J. Walker, R. Panciera, M. Escorihuela, and T. Jackson, "Assessing the smos soil moisture retrieval parameters with high-resolution nafe'06 data," *Geoscience and Remote Sensing Letters*, vol. 6, no. 4, pp. 635–639, 2009.

[64] J. Wigneron, A. Chanzy, Y. Kerr, H. Lawrence, J. Shi, M. Escorihuela, V. Mironov, A. Mialon, F. Demontoux, P. de Rosnay, and K. Saleh-Contell, "Evaluating an improved parameterization of the soil emission in l-meb," *IEEE Transactions on Geoscience and Remote Sensing*, vol. 49, no. 4, April 2011.

[65] P. Ferrazzoli, L. Guerriero, and J.-P. Wigneron, "Simulating l-band emission of forests in view of future satellite applications," *IEEE Transactions on Geoscience and Remote Sensing*, vol. 40, no. 12, pp. 2700–2708, December 2002.

[66] A. Van de Griend and J.-P. Wigneron, "The b-factor as a function of frequency and canopy type at h-polarization," *IEEE Transactions on Geoscience and Remote Sensing*, vol. 42, no. 4, pp. 786–794, April 2004.

[67] M. Schwank, C. Mätzler, M. Guglielmetti, and H. Flühler, "L-band radiometer measurements of soil water under growing clover grass," *IEEE Transactions on Geoscience and Remote Sensing*, vol. 43, no. 10, pp. 2225–2237, October 2005.

[68] J.-P. Wigneron, A. Chanzy, J.-C. Calvet, A. Olioso, and Y. Kerr, "Modeling approaches to assimilating l-band passive microwave observations over land surfaces," *Journal of Geophysical Research*, vol. 107, no. D14, pp. ACL11–1–14, 2002, atmosphere.

[69] J. Wang, P. O'Neill, T. Jackson, and E. Engman, "Multi-frequency measurements of the effects of soil moisture, soil texture, and surface roughness," *IEEE Transactions on Geoscience and Remote Sensing*, vol. GE-21, no. 1, pp. 44–51, January 1983.

[70] U. Wegmüller and C. Mätzler, "Rough bare soil reflectivity model," *IEEE Transactions on Geoscience and Remote Sensing*, vol. 37, no. 3, pp. 1391–1395, May 1999.

[71] M. Escorihuela, A. Chanzy, J. Wigneron, and Y. Kerr, "Effective soil moisture sampling depth of l-band radiometry: A case study," *Remote Sensing of Environment*, vol. 114, pp. 995–1001, 2010.

[72] P. de Rosnay, J.-C. Calvet, Y. Kerr, J.-P. Wigneron, F. Lemaître, M. Escorihuela, J. Muñoz Sabater, K. Saleh, J. Barrié, G. Bouhours, L. Coret, G. Cherel, G. Dedieu, R. Durbe, N. Fritz, F. Froissard, J. Hoedjes, A. Kruszewski, F. Lavenu, D. Suquia, and P. Waldteufel, "Smosrex: A long term field campaign experiment for soil moisture and land surface processes remote sensing," *Remote Sensing of Environment*, vol. 102, pp. 377–389, 2006.

[73] A. Mialon, J.-P. Wigneron, P. de Rosnay, M. Escorihuela, and Y. Kerr, "Evaluating l-meb from long term microwave measurements over a rough field, smosrex 2006," *Transactions on Geoscience and Remote Sensing*, vol. This Issue, In Prep, special issue on "SMOS - instrument performance and first results".

[74] C. Ruediger, J. P. Walker, and Y. H. Kerr, "On the airborne spatial coverage requirement for microwave satellite validation," *Geoscience and Remote Sensing Letters*, In Press.

TABLE I

AVERAGE THETAPROBE READINGS (RECALIBRATED BY MEANS OF SENSOR-SPECIFIC CURVES) AND CORRESPONDING STANDARD DEVIATIONS OF THE MINERAL SOIL FOR ALL RESPECTIVE CAMPAIGN DATES AND PATCHES.

	Agriculture		Heath		Forest	
	Avg.	Std.	Avg.	Std.	Avg.	Std.
29/04	0.146	0.031	0.237	0.075	0.184	0.075
02/05	0.151	0.033	0.235	0.069	0.168	0.07
04/05	0.142	0.026	0.232	0.073	0.162	0.06
09/05	0.167	0.027				

TABLE II

AVERAGE AND STANDARD DEVIATION OF VEGETATION WATER CONTENT [KG/M^2] ESTIMATED FOR DIFFERENT LAND COVER TYPES ON APRIL 28 AND MAY 6, RESPECTIVELY.

		28/04		06/05	
		Avg.	Std.	Avg.	Std.
Agriculture	Spring barley	0.014	0.004	0.102	0.044
	Winter barley	0.519	0.11	1.105	0.152
	Grass	0.913		0.216	
Heath	Natural grass	0.338	0.222	0.622	0.417
	Scotch heather	0.496	0.308	0.703	0.3
	Scotch heather/grass	0.335	0.088	0.55	0.139

TABLE III

L-MEB PARAMETERS INDIVIDUALLY ADJUSTED AS FUNCTION OF VEGETATION TYPE: MOST LIKELY VALUE 'UNI'(MIN-MAX VALUE RANGE). DUE TO THE NORTH-SOUTH RADIOMETER MEASUREMENT DIRECTION 'PARALLEL'/'ORTHOGONAL' POTATO BARE FIELDS IMPLY NORTH-SOUTH/EAST-WEST ROW ORIENTATIONS, RESP.

		LC	MODEL	S_D	H_R	VWC	b	τ_{NAD}
Bare field		166	FNO		0.39(0.15-0.58)			0
Potato field bare parallel		166	FNO	9.76 (0.85)	0.39(0.15-0.58)			0
Potato field bare orthogonal		166	FNO	63.51 (5.80)	1.15(1.12-1.17)			0
Spring cereal	29/04	166	FNO	10.64 (4.99)	0.39(0.15-0.58)	0.021(0.014-0.028)	0.11(0.08-0.15)	0.002(0.001-0.004)
	02/05					0.054(0.032-0.076)		0.006(0.003-0.011)
	04/05					0.076(0.044-0.108)		0.008(0.004-0.016)
	09/05					0.131(0.074-0.189)		0.014(0.006-0.028)
Winter cereal	29/04	166	FNO		0.39(0.15-0.58)	0.564(0.451-0.677)	0.11(0.08-0.15)	0.062(0.036-0.102)
	02/05					0.786(0.657-0.915)		0.086(0.053-0.137)
	04/05					0.934(0.795-1.074)		0.103(0.064-0.161)
	09/05					1.305(1.138-1.472)		0.144(0.091-0.221)
Agriculture grass		166	FNO		0.39(0.15-0.58)	0.565(0.216-0.913)	0.12(0.1-0.3)	0.068(0.022-0.274)
Trees		211	FFO		1.1(1.0-1.2)			0.65(0.2-1.0)
Coniferous forest		211	FFO		1.1(1.0-1.2)			0.65(0.2-1.0)
Forest clearing		166	FNO		1.1(1.0-1.2)			0
Young forest		166	FNO		1.1(1.0-1.2)			0.3(0.2-0.6)
Natural grass	29/04	166	FNO		0.8(0.5-1.1)	0.360(0.123-0.598)	0.12(0.1-0.3)	0.043(0.012-0.179)
	02/05					0.468(0.156-0.779)		0.056(0.016-0.234)
	04/05					0.539(0.179-0.900)		0.065(0.018-0.270)
	09/05					0.719(0.235-1.202)		0.086(0.024-0.361)
Scotch heather	29/04	166	FNO		0.8(0.5-1.1)	0.512(0.205-0.819)	0.12(0.1-0.3)	0.061(0.020-0.246)
	02/05					0.591(0.286-0.895)		0.071(0.029-0.268)
	04/05					0.643(0.341-0.945)		0.077(0.034-0.284)
	09/05					0.774(0.477-1.071)		0.093(0.048-0.321)
Scotch heather/grass	29/04	166	FNO		0.8(0.5-1.1)	0.351(0.259-0.443)		0.042(0.026-0.133)
	02/05					0.433(0.322-0.544)		0.052(0.032-0.163)
	04/05					0.488(0.364-0.611)		0.059(0.036-0.183)
	09/05					0.624(0.468-0.780)		0.075(0.047-0.234)

TABLE IV

RMSE AVERAGED OVER INDIVIDUAL PATCH TYPE AND RADIOMETER CONFIGURATIONS AND OVER ALL (AVG/STD ALL CONFIG); AVG.(STD.) FOR ALL RUNS WITH N_{RH}=2/0 AND N_{RV}=0/-1, RESP.

	AVG(STD) All RUNS	
N_{RH}/N_{RH}	2/0	0/-1
AVG 0H	17.60(11.50)	17.60(11.50)
AVG 0V	17.15(11.42)	17.15(11.42)
AVG 40H	34.49(13.32)	22.52(13.77)
AVG 40V	10.49(7.65)	8.57(6.57)
AVG Agricult	21.98(11.46)	18.22(11.18)
AVG Forest	17.15(9.56)	14.07(9.21)
AVG Heath	20.66(11.59)	17.07(11.35)
AVG(STD) All CONFIG	19.93(10.82)	16.46(10.55)

TABLE V

DESCRIPTION OF 7 BEST-FIT AND 'AVG.' (REF) MODEL RUNS INCL. RMSE AVG.(STD.) OVER ALL PATCH TYPE AND RADIOMETER CONFIGURATIONS. SM: SOIL MOISTURE, BD: BULK DENSITY, S: SAND, C: CLAY, HR: ROUGHNESS PARAMETER, TAU: NADIR OPTICAL DEPTH

Model run		RMSE All Avg.(Std.)	
Description	Rank	$N_{RH}2N_{RH}0$	$N_{RH}0N_{RH}$-1
Smmin_BDmax_SminCmax_HRmax_TAUmax	1	5.91(4.81)	4.02(2.63)
Smmin_BDmin_SminCmax_HRmax_TAUmax	2	5.98(3.4)	4.48(2.93)
Smmin_BDmin_SminCmax_HRmax_TAUmin	3	6.65(6.43)	4.37(2.77)
Smmax_BDmin_SminCmax_HRmax_TAUmax	4	6.9(6.73)	4.37(2.44)
Smmin_BDmax_SminCmax_HRmax_TAUmin	5	7.35(7.58)	4.76(2.56)
Smmax_BDmax_SminCmax_HRmax_TAUmax	6	8.02(7.39)	5.19(2.37)
Smmax_BDmin_SminCmax_HRmax_TAUmin	7	9.65(9.17)	6.37(2.70)
Smavg_BDind/avg_SavgCavg_HRuni_TAUuni	Ref	17.16(10.31)	13.08(6.69)
Avg. All Runs		19.93(10.82)	16.46(10.55)

TABLE VI

SIMPLE AND WEIGHTED AVERAGE (STANDARD DEVIATION) OF EMIRAD-2 BRIGHTNESS TEMPERATURES [K] FOR SMOS PIXEL AROUND GRID NODE 2002029, H AND V-POLARIZATIONS, 0 AND 40° INCIDENCE ANGLES, RESP.

	0 H		0 V		40 H		40 V	
	Simple	Weighted	Simple	Weighted	Simple	Weighted	Simple	Weighted
29/04	249.03(6.75)	248.88(4.29)	248.85(6.66)	248.67(4.22)	238.35(7.23)	238.46(4.62)	257.55(5.08)	257.55(2.71)
02/05	244.11(6.93)	243.86(4.33)	243.96(6.96)	243.73(4.35)	234.13(7.88)	233.96(5.35)	252.95(5.22)	252.83(3.06)
04/05	248.13(6.12)	248.03(3.64)	247.95(6.08)	247.82(3.59)	238.73(6.57)	238.66(3.98)	255.66(4.78)	255.6(2.36)
09/05	244.87(7.14)	244.8(4.21)	244.9(7.02)	244.81(4.19)	235.55(8.14)	235.6(5.26)	253.8(5.08)	253.8(2.76)

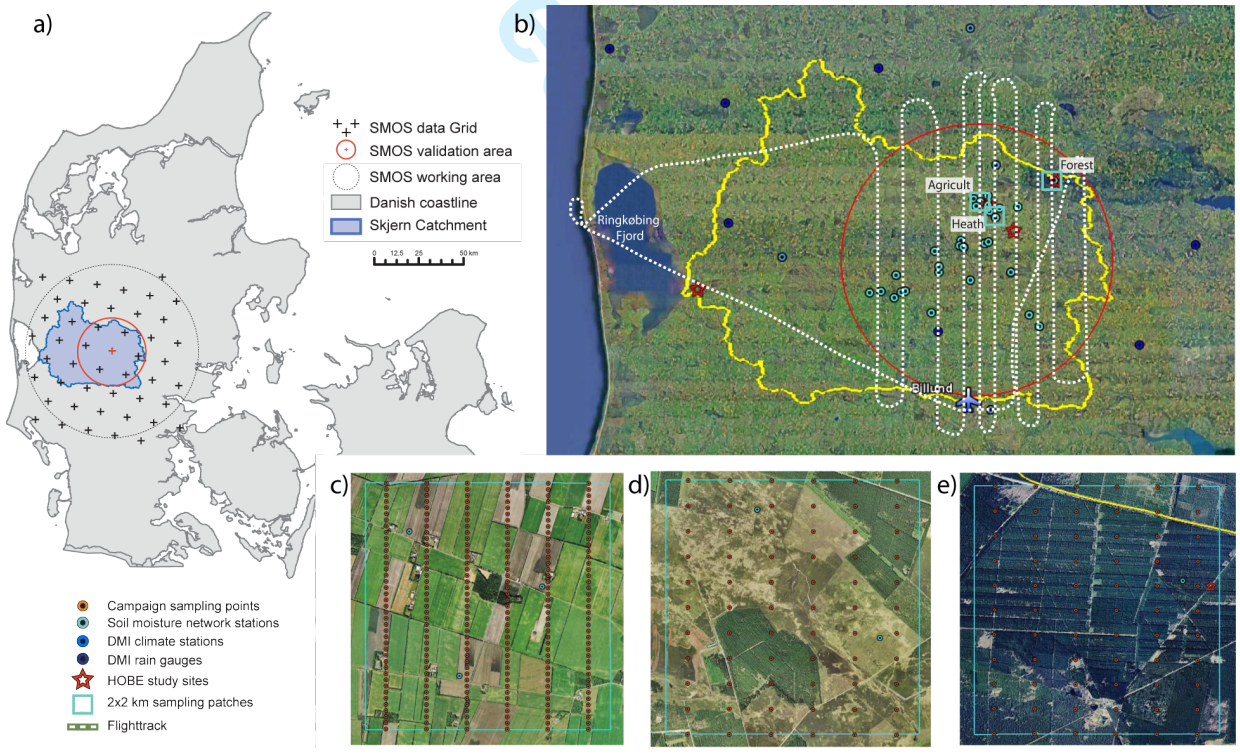

Fig. 1. Area overview. a) Danish coastline, Skjern River Catchment and SMOS validation site around grid node 2002029 including the SMOS 'working area', b) campaign flight tracks and sampling patches, network stations, DMI rain gauges and HOBE sites, c) agriculture, d) heath, and e) forest campaign ground sampling transects

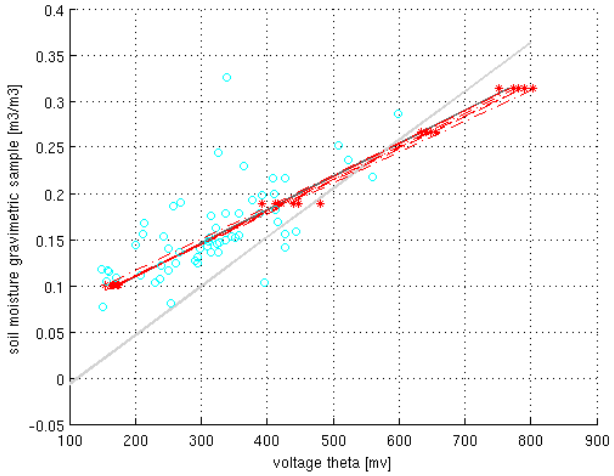

Fig. 2. Manufacturer Theta default curve for mineral soils (grey -), and sensor- and site-specific linear Theta calibration curves (red – and black -) derived from lab measurements (red ∗) and validated with gravimetric field samples (blue ○) at the example of agricultural mineral soil.

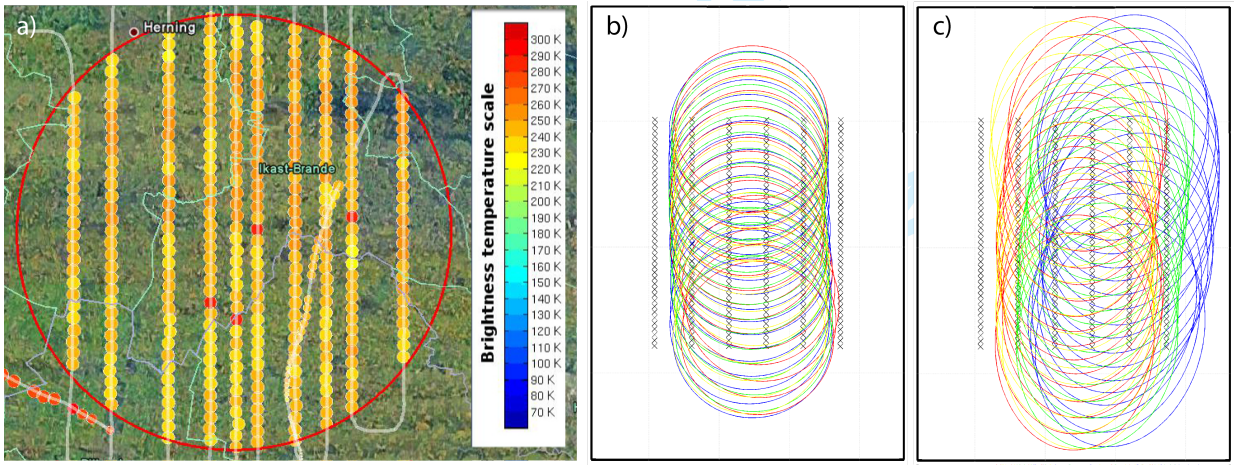

Fig. 3. a) EMIRAD-2 data coverage of SMOS pixel around grid node 2002029 (0° H-pol 02. May) and agriculture 2x2 km ground patch b) 0° and c) 40° antenna, respectively. Blue: 29. April, red: 02. May, green: 04. May, yellow: 09. May.

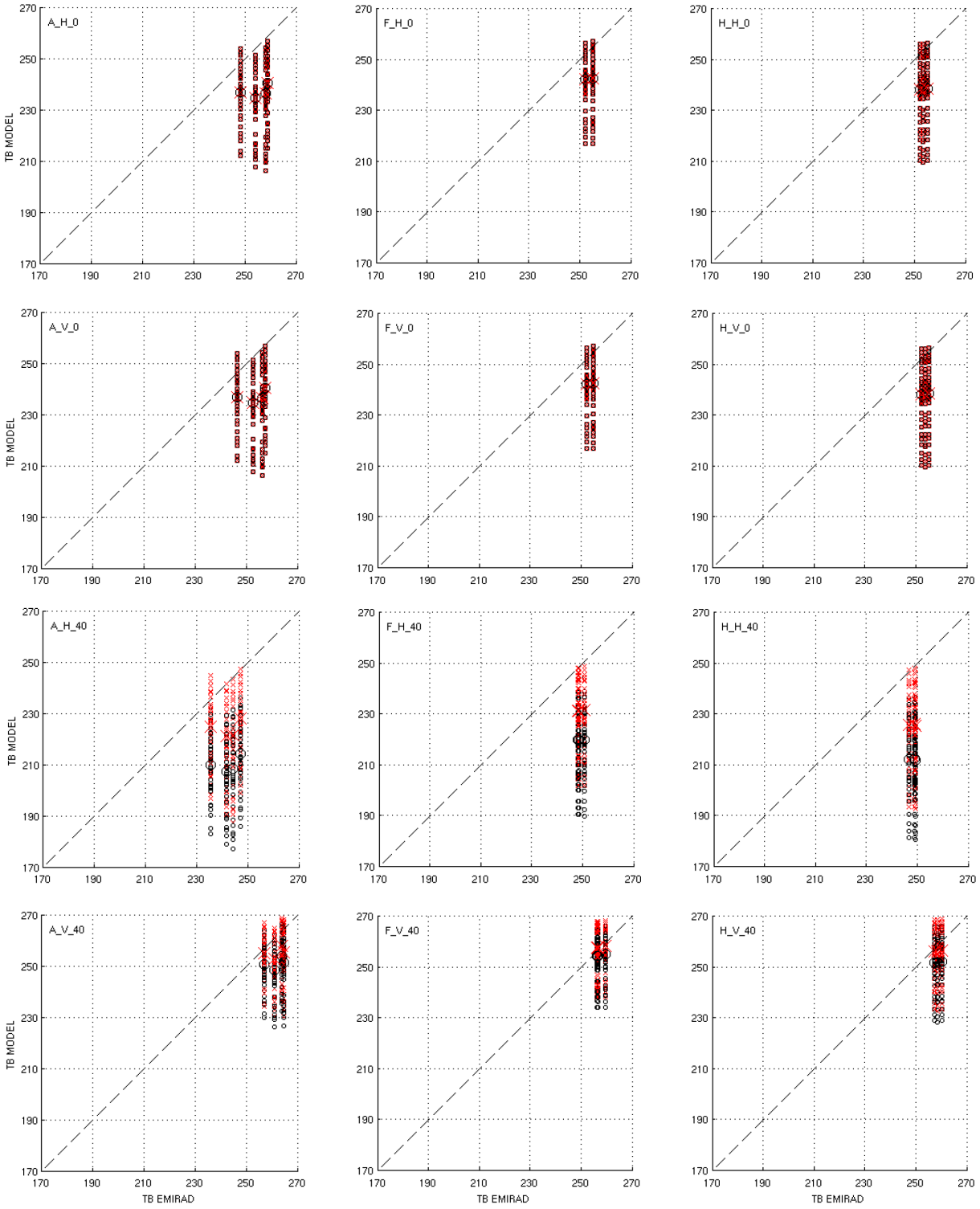

Fig. 4. Modeled ground data vs. EMIRAD T_B, different runs using all possible combinations of min./max. values for 5 selected parameters with N_{RH}/N_{RV}=2/0 (black ○) and N_{RH}/N_{RV}=0/-1 (red x) incl. 'avg.-run' (black ◯/red X) for all patch types (first labeling letter of individual plots: Agriculture, Forest, and Heath), sampling dates, H and V pol. (second labeling letter), and 0 and 40° θ (number in labels), resp.

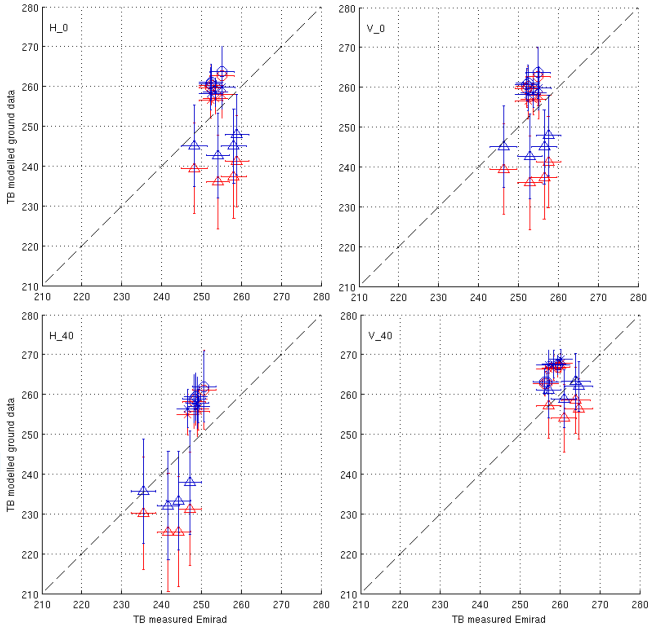

Fig. 5. Modeled ground data vs. EMIRAD T_B with site-specific soil texture data (red) vs. soil texture info from Danish topsoil grid (blue) for H and V pol., 0 and 40° θ, all sampling dates and patch types, resp.: agriculture (△), forest (◯), heath (X); avg. % sand and clay, max. H_R and τ_{NAD}, avg. soil moisture, dry bulk density estimated at individ. locations or patch avg., and N_{RH}=0/N_{RV}=-1

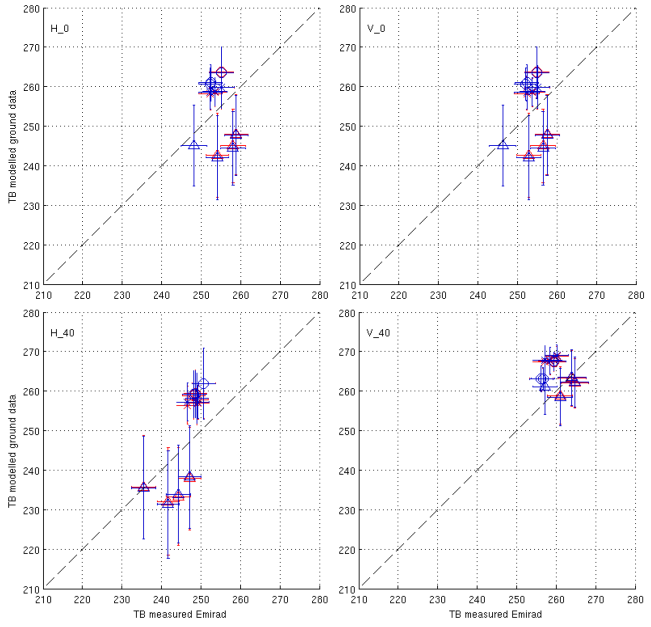

Fig. 6. Modeled ground data vs. EMIRAD T_B averaged by simple (red) vs. weighted (blue) mean for H and V pol., 0 and 40° θ, all sampling dates and patch types, resp.: agriculture (△), forest (◯), heath (X); avg. % sand and clay, max. H_R and τ_{NAD}, avg. soil moisture, dry bulk density estimated at individ. locations or patch avg., and N_{RH}=0/N_{RV}=-1

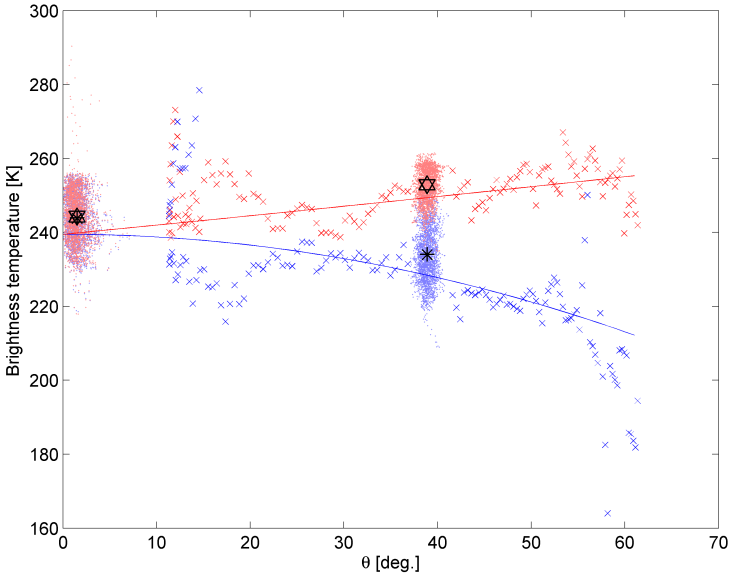

Fig. 7. EMIRAD-2 data averaged over all 10 flight tracks and SMOS L1C TOA (ascending overpass) data of DGG node 2002029 on May 02. Blue/red x: SMOS T_B H/V, blue/red -: SMOS curve fit H/V, blue/red clusters: EMIRAD-2 T_B H/V, black +/x: EMIRAD-2 T_BH simple/weighted mean, black ∇/$\triangle$: EMIRAD-2 T_BV simple/weighted mean.